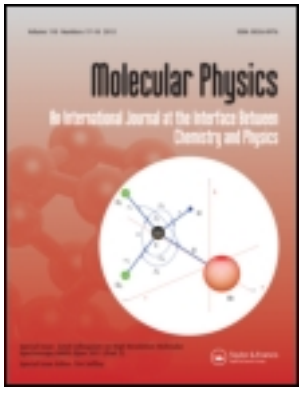

Molecular Physics: An International Journal at the Interface Between Chemistry and Physics

Publication details, including instructions for authors and subscription information:
http://www.tandfonline.com/loi/tmph20

Experimental 2CH excitation in acetylene-containing van der Waals complexes

K. Didriche [a] , T. Földes [a] , C. Lauzin [a] , D. Golebiowski [a] , J. Liévin [a] & M. Herman [a]

[a] Laboratoire de Chimie quantique et Photophysique, Université libre de Bruxelles, Bruxelles, Belgium

Accepted author version posted online: 25 Jun 2012.Version of record first published: 16 Jul 2012.

To cite this article: K. Didriche , T. Földes , C. Lauzin , D. Golebiowski , J. Liévin & M. Herman (2012): Experimental 2CH excitation in acetylene-containing van der Waals complexes, Molecular Physics: An International Journal at the Interface Between Chemistry and Physics, 110:21-22, 2781-2796

To link to this article: http://dx.doi.org/10.1080/00268976.2012.705347

Molecular Physics
Vol. 110, Nos. 21–22, November 2012, 2781–2796

Taylor & Francis
Taylor & Francis Group

SPECIAL ISSUE: FASE (FEMTO-, ASTRO-, SPECTRO-ETHYNE)

Experimental 2CH excitation in acetylene-containing van der Waals complexes

K. Didriche#§, T. Földes#‡, C. Lauzin#, D. Golebiowski†, J. Liévin and M. Herman*

Laboratoire de Chimie quantique et Photophysique, Université libre de Bruxelles, Bruxelles, Belgium

(*Received 24 May 2012; final version received 15 June 2012*)

Spectroscopic results are presented concerning the 2CH excitation around 1.5 μm in van der Waals complexes of acetylene (C_2H_2) with Ar, Kr, N_2, CO_2, N_2O and C_2H_2. Many are reviewed from the literature, with some updates. Previously unpublished results are also presented, concerning the mechanism of formation of C_2H_2–Ar in the supersonic jet, the assignment of new spectral structures in C_2H_2–N_2O, and the first observation of 2CH excitation in C_2H_2–Ne, C_2H_2–H_2O, C_2H_2–D_2O and $(C_2H_2)_n$. Lifetimes of these 2CH vibrationally excited dimers are discussed.

Keywords: van der Waals complexes; acetylene; overtone spectroscopy; supersonic expansion; cavity ring-down spectroscopy

1. Introduction

Spectroscopic research of van der Waals species under high-resolution probably started in the 1960s, notably with the observation of bound states of the H_2 dimer in a cold cell [1]. These pioneering works opened the way to high-resolution spectroscopy in the microwave and infrared spectral ranges [2–5]. It proved to be a challenging field, experimentally because these weakly bound species are difficult to produce with sufficient density, and theoretically because these complexes show large amplitude motions. This field remained active [6–11], with recently renewed interest due to more stringent potential astrophysical and planetary relevance [12–16]. In the overtone vibrational range all previously highlighted challenges are magnified and therefore only few experimental studies were reported in the literature, such as of HF–Ar [17,18], $(HF)_2$ [19–22], $(HCN)_2$ [23], $(H_2O)_2$ [24], $(N_2O)_2$ [25], C_6H_6–Ar [26], OH–Ar [27], N_2–HF [28], OC–HF [29] and H_2–Ar [30].

Over recent years, the Brussels group has built an experimental set-up merging a powerful free supersonic jet and ultrasensitive high-resolution optical detection [31,32]. It uses two large turbomolecular pumps and a continuous-wave cavity ring-down diode laser spectrometer (CW-CRDS) [33,34]. The diode laser sources emit in the 1.5 μm range, corresponding to 2CH excitation in C_2H_2. The related monomer absorption band is $\nu_1 + \nu_3$, with modes 1 and 3, the symmetric and antisymmetric CH normal modes, respectively [35]. The expertise of the Brussels group in acetylene overtone spectroscopy [36,37] naturally induced jet-cooled experiments on this species, as an initial test target. They unexpectedly led to the observation of C_2H_2–Ar, in 2007 [38]. Sharp sub-Doppler lines from this species were indeed not expected, since the 2CH excitation energy is about 60 times higher than the van der Waals bonding energy of the C_2H_2–Ar complex, therefore it is expected to be dissociated. Searching the literature revealed a previous, low-resolution literature report on this band [39]. More acetylene-containing complexes have since been observed relying on the same 2CH monomer excitation band, while the performance of the experimental set-up was continuously improved over the years. Challenging theoretical, *ab initio* based research was also stimulated by these observations, however this is not reviewed in this paper [40].

The families of acetylene-containing van der Waals complexes for which experimental results were produced in the 2CH excitation range, around 1.5 μm, are illustrated in Figure 1. Besides the early report of C_2H_2–Ar by Orr and coworkers already mentioned [39], the only results on 2CH overtone spectra in acetylene-containing van der Waals species seem to arise from the Brussels group, thus essentially limiting the directly

*Corresponding author. Email: mherman@ulb.ac.be
first authors in alphabetic order.
§ FRS-FNRS postdoctoral fellow.
‡ AGACC postdoctoral fellow.
† FRIA PhD student.

ISSN 0026–8976 print/ISSN 1362–3028 online

http://dx.doi.org/10.1080/00268976.2012.705347
http://www.tandfonline.com

relevant references hereafter to self-citations. Some of the literature on experiments in lower energy spectral ranges and on theoretical investigations will also be mentioned, for completeness. Most of the high-resolution analyses we report on were performed using a rigid rotor model [41], exploiting the very convenient PGOPHER software [42]. We are also updating here some of the literature results and discussions. Furthermore, still unpublished and new, recent experimental results are also included in this paper.

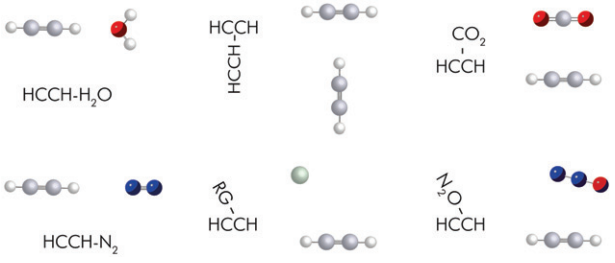

Figure 1. Families of van der Waals complexes observed in the 2CH excitation spectral range (RG: Rare Gas).

The next section details the evolution of the experimental set-up we have used. Results are then presented, starting with acetylene–rare gases (RG) in Section 3, namely C_2H_2–Ar, C_2H_2–Ne and C_2H_2–Kr. Section 4 continues with acetylene–diatomic/triatomic (AB/ABC) species, including C_2H_2–N_2, C_2H_2–H_2O, C_2H_2–D_2O, C_2H_2–N_2O and C_2H_2–CO_2. Section 5 concerns C_2H_2–C_2H_2 and larger multimers. Additional results from C_2H_2–Ar are presented in Section 6 and linewidths are discussed in Section 7, before concluding.

2. Description of FANTASIO(+)

The set-up in Brussels is named FANTASIO+ [32] where FANTASIO stands for "**F**ourier tr**AN**sform, **T**unable diode and quadrupole m**A**ss spectrometers interfaced to a **S**upersonic expans**IO**n" and the + for the different updates since the initial report, in 2007 [31]. We also sometimes refer to FANTASIO(+) whenever spectra of a species were initially recorded using FANTASIO and later using its improved version, FANTASIO+. The CRDS spectrometer and the free jet expansion are shown schematically in Figure 2 and described in this section.

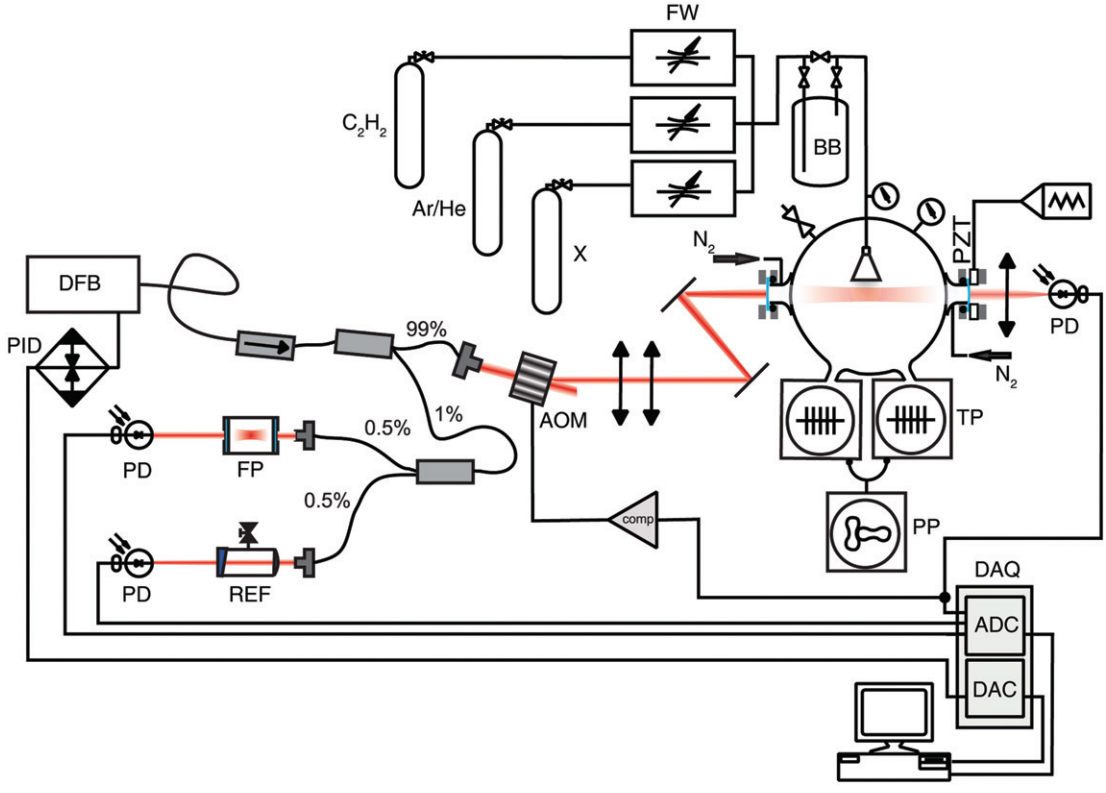

Figure 2. Scheme of the experimental set-up. DFB, distributed feedback laser diode; PID, proportional–integral–derivative temperature controller; PD, photodiode; AOM, acousto-optic modulator; comp, comparator; FP, Fabry–Pérot interferometer; REF, reference cell; FW, flowmeter; BB, bubbler; PZT, high-voltage piezo stack ring; TP, turbo pumps; PP, primary pump; DAQ, data acquisition card, with ADC, analog-to-digital converter and DAC, digital-to-analog converter; X, high pressure bottle of a third gas, either a second carrier rare gas or the molecule to form the partner in the acetylene complex.

2.1. *Free jet expansion*

The free supersonic jet expansion in FANTASIO+ is produced using two identical, large turbomolecular pumps (Leybold MAG W3200 CT; 2850 l/s), rather than one initially. They are Teflon coated and backed by an Alcatel ADS 860 HII group. Both turbomolecular units are directly mounted below the cylindrical expansion cell, about 32 cm in diameter. The Y connection matches the identical pump and cell diameters. The reservoir (p_0) and residual (p_∞) pressures are measured using MKS Baratron gauges (1000 and 1 torr full scale, respectively).

The acetylene and carrier gas flows are measured using MKS and Brooks flowmeters (10 000 and 50 000 sccm full scale, respectively, where sccm denotes cubic centimeter per minute at standard conditions for temperature and pressure). The reservoir pressure is currently typically 100 kPa, as opposed to 50 kPa initially, for similar residual pressures, of the order of 1 Pa. Spectra of C_2H_2–Ar recorded with one and two turbomolecular pumping units are shown in panels (a) and (b) of Figure 3, respectively. The comparison demonstrates an increase of a factor 2 in the S/N. A more reflective mirror set is used for the spectrum presented in panel (c), as further discussed below. As a rule, experimental conditions are not repeated in the legends of figures presenting spectra that are adapted from the literature, as for Figure 3. Also, the strongest lines on the spectra are almost always due to acetylene monomer absorption and are not included in the simulated data whenever presented.

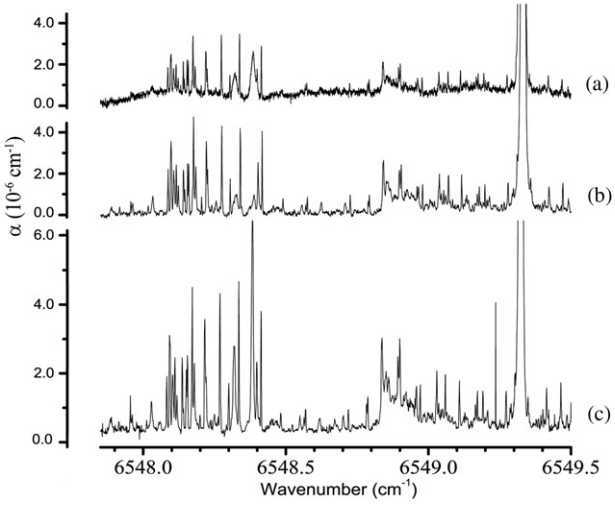

Figure 3. CW-CRDS jet-cooled spectrum of a mixture of C_2H_2 and Ar recorded in the 2CH acetylenic excitation range using FANTASIO(+). The initial FANTASIO set-up was used for the spectrum presented in panel (a); then improved using first a second turbomolecular pump, in panel (b); next, in panel (c), with FANTASIO+, using a more reflective set of mirrors. The intensity scale was multiplied by a factor 1.5 in panel (c) to achieve a noise level visually similar to that in panel (b) and to highlight the corresponding gain in the S/N level. Adapted from [32].

Thanks to the use of two turbo pumps, helium and neon could be used as carrier gases, in addition to argon, while these gases were overriding the pump capacity previously. This wider range of experimental conditions proved to be crucial, especially for investigating the acetylene dimer.

2.2. *CW-CRDS spectrometer*

The general features of the CW-CRDS spectrometer are directly inspired from the developments by Romanini and coworkers [43,44]. Distributed feedback (DFB) tunable diode lasers (TDL) emitting in the 1.5 μm range (e.g. ILX lightwave, 1 MHz linewidth) are used. The TDL beam is sent through an optical isolator (Thorlabs 4015 5AFC-APC) and then split by two fibre-optical beam splitters used to direct about 0.5% of the laser beam into a home-made Fabry–Pérot interferometer made of two 50% reflectivity flat mirrors mounted on an Invar bar, and another 0.5% to a reference cell. These two components will be detailed later in the calibration section. The remaining 99% of the light is focused by a fibre collimation package ($f = 4.5$ mm) onto an acousto-optical modulator (AOM) from AA Opto-Electronic (MGAS 80-A1). The first-order diffraction from the AOM is injected into the TEM_{00} mode of a linear ring-down cavity through two lenses ($f_1 = 30$ mm, $f_2 = 50$ mm) and two steering mirrors. The cavity is composed of two wedged plano-concave mirrors (radius = 1000 mm), separated by about 540 mm. The output mirror is mounted on a piezo actuator (Piezomechanik HPST 1000/15-8/5). The light exiting the cavity is focused through a lens ($f = 150$ mm) on a photodetector.

For ring-down detection, the PZT is driven at a selected frequency (typically 500 Hz) and cavity mode matching with the laser is achieved at twice the selected frequency. The AOM is triggered to turn off as soon as the light intensity exiting the cavity exceeds a threshold value. The same event triggers the measurement procedure of the ring-down signal.

The ring-down decays are sampled by a PCI-6251 multifunction data acquisition (DAQ) card, with a 16 bit, 1.5 MHz analog-to-digital converter. The acquisition is PC driven by home-made software developed using LabView. A robust Levenberg–Marquardt algorithm (LMA) [45] developed in C programming language is used for ring-down transient fitting,

embedded as a subroutine into a LabView program. The TDL frequency can be tuned by changing the TDL temperature using a home-made PID stabilizer controlled by the DAQ card. The temperature tuning from about 60°C to −5°C corresponds approximately to a $30\,cm^{-1}$ tuning range. The resolution can be adapted during the experiment by adjusting the temperature step.

The absorption coefficient α is directly calculated using

$$\alpha = \frac{L}{cl}\left(\frac{1}{\tau} - \frac{1}{\tau_0}\right) \approx \frac{L}{cl}\left(\frac{\Delta\tau}{\tau_0^2}\right) \quad (1)$$

where c is the speed of light, L and l the length of the resonant cavity and of the absorption cell, respectively, and τ and τ_0 the ring-down times measured with and without the sample, respectively. The minimum absorption coefficient

$$\alpha_{min} \approx \left(\frac{1-R}{l}\right)\frac{\Delta\tau_{min}}{\tau_0} \quad (2)$$

where R is the mirror reflectivity, can be improved by N-fold averaging (within some limitations) and the sensitivity is then defined as:

$$\alpha_{min} \approx \frac{L}{cl}\frac{\sqrt{2}\Delta\tau_{min}}{\sqrt{N}\tau_0^2} \quad (3)$$

where N is the number of averaged ring-down times, usually 50–200.

2.3. *FANTASIO+*

Besides the second turbo pump, the most significant update in FANTASIO+ is the typical ring-down time, which was increased from 15 to some 130 µs using a new set of mirrors (Layertec 106767), with $R = 99.9985\%$. The number of passes in the 540 mm long cavity has increased from about 8300 previously to 70 000. When using a 1 cm long slit (about 30 µm wide), as in the present version of FANTASIO+, the effective absorption path in the cooled gas is 700 m. As a result of the very high reflectivity of the new cavity mirrors, the typical light power leaking out of the cavity has significantly decreased, requiring a new detection system using a PIN photodiode in photoconductive mode amplified by a three-stage readout circuit [46].

The overall gain in S/N between FANTASIO and FANTASIO+, comparing regular operational conditions, is about 10. The present α_{min} has been measured to be $5 \times 10^{-10}\,cm^{-1}$ for typically 500 ring-down averaged per spectral point in about 2 seconds.

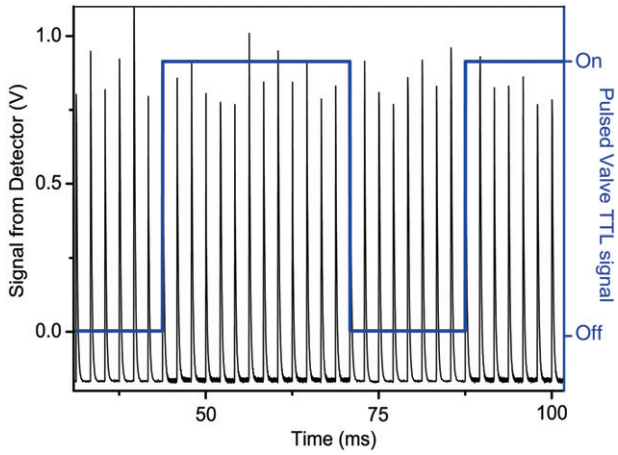

Figure 4. Typical sequence of ring-down events in black (left y-scale) and pulsed valve opening, in blue (right y-scale), in FANTASIO+ (see text for details).

The corresponding α_{min} is $2.7 \times 10^{-8}\,cm^{-1}$ when probing the supersonic expansion over 1 cm.

Recently, pulsed operation was made possible. Because mechanical noise causes significant random jitter in the ring-down event occurrence, synchronization is problematic and greatly hinders repetition rate. Our solution is based on not synchronizing the pulsed valve to the ring-down events. The gas pulse repetition frequency and duty cycle can be set conveniently to the limit determined by the pumping system. The state of the pulsed valve is then recorded with every ring-down event, as illustrated in Figure 4. The ring-down transients are sorted based on this information. On-pulse and off-pulse (used as "real-time baseline") ring-down times are easily recovered.

2.4. *Calibration procedure*

The line position calibration procedure uses a cell typically filled with 25 hPa of C_2H_2. This reference cell is composed of a $\varnothing = 1''$, 15 cm focal distance plano-convex lens and a 2° round wedge prism glued to a 10 cm long $\varnothing = 2$ cm stainless steel tube. One face of the tube is cut at a small angle to avoid parallel optical surfaces. There is a $1/4''$ tube with a valve welded to the side of the reference cell to fill it. For linearization of the spectra a Fabry–Pérot interferometer is used, which is composed of two planar 50% reflectivity mirrors mounted on an $\varnothing = 2$ cm invar alloy rod. The length of the interferometer is about 15 cm (corresponding to a free spectral range of ~1 GHz, ~$0.033\,cm^{-1}$). Two fibre-optical beam splitters are used to direct about 0.5% of the laser radiation to the interferometer and 0.5% to the reference cell. The

radiation is coupled to the reference cell and the interferometer by fibre collimation lenses. The transmittance of the reference cell is monitored by an InGaAs PIN photodiode in photoconductive mode powered by two 9 V batteries. The transmittance of the interferometer is monitored using a similar photodiode. All optics are anti-reflective coated. CRDS spectra, transmittance spectra of the reference cell and transmittance of the interferometer are simultaneously recorded during a scan. A LabView calibration routine developed by P. Čermák is used [47]. The positions of the maxima in the interferometer transmittance are fitted with a smooth partial polynomial fit and used for linearization of the wavelength scale with an initial offset and free spectral range (FSR) setting. A peak detector algorithm based on quadratic polynomial fits is used to detect peaks in the reference cell spectra. It displays the difference between positions of the detected peaks on the linearized wavelength scale and supplies reference stick spectra. Offset and FSR corrections can be manually introduced to minimize residuals. One point in the spectrum can be fixed in relation to the FSR correction so as to be able to "lock" one peak to a reference position while still allowing for linear transformations. We could reproduce literature values [48,49] within $\pm 5 \times 10^{-4}\,\mathrm{cm}^{-1}$. The measurement accuracy is better for shorter scans.

After calibrating a CRDS spectrum from such reference measurements, an additional offset correction is typically introduced to compensate for shifted and asymmetric line shapes. Such problems arise mainly from the flow asymmetry and deviation from ideal orthogonal interaction between the jet and the laser beam [50]. Even though this offset correction relies on determining the center of saturated and asymmetric lines, good agreement, within $\pm 5 \times 10^{-4}\,\mathrm{cm}^{-1}$, was found when cross-checking the calibration with unsaturated $^{12}CH^{13}CH$ line positions from [51], recorded in natural abundance in the supersonic expansion. On this basis, we claim accuracy better than $\pm 1 \times 10^{-3}\,\mathrm{cm}^{-1}$. This is a major improvement compared to the initial FANTASIO set-up by about one order of magnitude, still to be improved.

3. Investigation of acetylene–RG complexes

In acetylene–RG complexes, the equilibrium geometry is skew, T-shaped [40]. Actually, the lighter the atomic RG mass, the less hindered the rotation of the RG around the acetylene structure. As further discussed below, the spectra of the acetylene–RG complexes we have investigated can, however, be reasonably well interpreted assuming an averaged T-shaped zero point geometry, thus with $\theta_0 = 90^\circ$ and R_0 slightly above 4 Å, as defined in Figure 5. The *a* and *b* principal axes are respectively perpendicular (and going through the RG atom) and parallel to the acetylene molecular axes. *b*-type selection rules are thus expected for the 2CH vibrational excitation, with ΔK_a and ΔK_c odd, and $\Delta J = 0, \pm 1$.

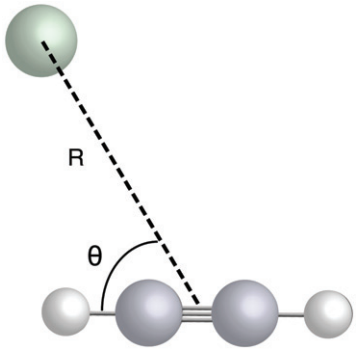

Figure 5. Jacobi (R, θ) coordinates for acetylene–RG van der Waals complexes.

3.1. *Argon*

C_2H_2–Ar presents a so-called pathologically flat potential energy surface, which has been extensively investigated by *ab initio* calculations [40,52–66], demonstrating the skew T-shaped *equilibrium* geometry, with $\theta_e = 60^\circ$ and $R_e = 4$ Å. Experimentally, the C_2H_2–Ar van der Waals molecular complex has been studied in various spectral regions, including microwave [67–69], infrared [56,68,70–74] and, as already mentioned, near-infrared [39].

We recorded the 2CH acetylenic excitation band using FANTASIO(+), with argon as carrier gas. The experimental results stimulated new *ab initio* calculations. Sub-bands with $K_a = 0 \leftarrow 1$, $1 \leftarrow 0$ and $2 \leftarrow 1$ were identified and many rotational lines assigned [38,66]. As discussed in these papers, many problems arose from attempts to perform a more detailed analysis, including succeeding in a global fit of all assigned data, reproducing relative intensity behavior, and also assigning weaker lines both close and away from the main structures. Most of these problems most likely arise from the non-rigid character of the complex.

A 1:3 intensity alternation is expected to occur between K_a values for a symmetric T-shaped r_0 structure. Such an alternation is transposed from the monomer even:odd J''-values to the dimer even:odd K_a''-structure, in the intensity ratio 1:3, respectively.

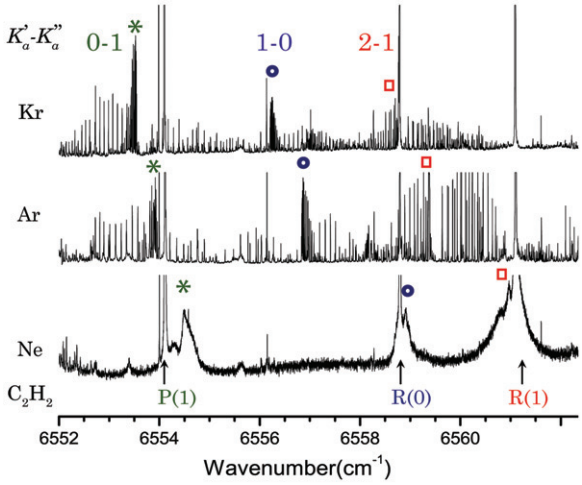

Figure 6. Comparison of CW-CRDS jet-cooled spectra of C_2H_2 recorded in the 2CH acetylenic excitation range using FANTASIO(+). Experimental conditions were optimized for C_2H_2–Kr (top), C_2H_2–Ar (middle) and C_2H_2–Ne (bottom). The previously unpublished C_2H_2–Ne van der Waals complex was generated by expanding C_2H_2/Ne 12/2190 sccm, p_0/p_∞ 306000/1 Pa through a 5×0.050 mm slit nozzle. The injector was cooled down to 268 K. Assigned sub-bands are identified and the various signs indicate the position of the related Q-branches. The top of the much stronger monomer line intensities was systematically erased. The lowest J monomer lines are also assigned at the bottom.

Slight discrepancies from this behavior were noticed when analyzing data, but attributed at the time to cooling mechanisms in the expansion affecting population distribution on K_a'' sub-states. The comparison with the $^{12}C_2H_2$–Kr spectrum, since recorded, presented in Figure 6 and further discussed below, currently contradicts this hypothesis. The 1:3 intensity alternation appears neatly with even:odd K_a'' in the latter complex. It is expected that the non-rigid character of the lighter complex is responsible for the departure of the 1:3 intensity alternation in $^{12}C_2H_2$–Ar; however, a more elaborated and still missing specific explanation is required.

3.2. *Krypton and xenon*

There seems to be only one published, empirical potential energy surface (PES) for C_2H_2–Kr and C_2H_2–Xe [65], and no *ab initio* one until recently [40]. There are no previously reported spectral data for these species, in any spectral range.

We searched for the 2CH acetylenic excitation band using FANTASIO(+), optimizing a mixture of argon and krypton as carrier gas. A structure very similar to that of C_2H_2–Ar was recorded, readily identified to be C_2H_2–Kr and already presented in Figure 6. The analysis confirmed the molecular carrier and thus produced the first rotational constants for C_2H_2–Kr [75]. They are, in cm^{-1}, $A = 1.56861$, $B = 0.051681(56)$ and $C = 0.048559(60)$, the former constrained to the C_2H_2–Ar value, from [69]. Because of this constraint we did not attempt retrieving lifetimes from the linewidth measurements, preventing this complex being among those further discussed in Section 4. We did not attempt to observe the heavier complex, requiring an unaffordable quantity of xenon to be purchased. This complex can, however, be expected to lead to similar spectra as recorded for C_2H_2–Kr and –Ar. Additional sub-bands can also be expected to be observable in C_2H_2–Kr using FANTASIO+, as for C_2H_2–Ar.

3.3. *Neon and helium*

Rotationally resolved infrared spectra of Ne–DCCH and broader spectral features attributed to Ne–HCCH have been reported in the literature [76], leading to an empirical PES. There are also microwave [77], and molecular beam scattering, pressure-broadened cross section data [65]. We searched for the 2CH acetylenic excitation band in Ne–HCCH using FANTASIO(+), optimizing a mixture of argon and neon as carrier gas. Lines could be observed only after cooling the nozzle injector to some −5°C using Peltier elements. This spectrum, also presented in Figure 6, has not previously been published. The rotational structure is not resolved and the K structure is tentatively assigned, with each K sub-band close to the monomer lines. It is based on the comparison with the other acetylene–RG complexes as well as, though not further detailed here, on the comparison with literature assignments in the 3 μm range [76]. More theoretical work is required to confirm the present, tentative assignments.

Concerning helium, different theoretical and experimental studies have been published, see e.g. [78–80], but no resolved infrared or microwave spectrum has yet been reported, except very recently for C_2D_2–He [81]. Our attempts to observe the related 2CH spectrum using FANTASIO+ have all failed, so far. Given the evolution of the spectral pattern from –Kr to –Ne, see Figure 6, a strong predissociation mechanism might occur upon 2CH acetylenic excitation in C_2H_2–He, which could possibly explain this lack of success. The decreasing stability of the acetylene–RG complexes with decreasing RG mass is confirmed by *ab initio* results, as discussed in [40].

4. Investigation of acetylene–AB/ABC complexes

Acetylene is known to make mixed dimers with a number of other molecular species. We have succeeded in observing some of them in the near-infrared range, and these are reported in this section.

4.1. N_2 and H_2O/D_2O

We searched for the 2CH acetylenic excitation bands in C_2H_2–N_2 and C_2H_2–H_2O/D_2O using FANTASIO(+). These species were already reported in the literature from spectra in the microwave range [82] and [83], infrared range [84–86] and [87–89], and characterized by *ab initio* calculations, [90] and [91,92], with the selected references provided for C_2H_2–N_2 (and other acetylene isotopologues) and C_2H_2–H_2O/D_2O, respectively. The related spectral analyses were successfully carried out in the literature assuming linear or pseudo-linear geometry, thus only including B principal rotational constants.

The near-infrared data we have recently recorded on C_2H_2–N_2 confirm the linear geometry and have produced original, 2CH–upper state constants now reported in the literature [93]. The upper state looks heavily perturbed.

Data on C_2H_2–H_2O/D_2O were very recently recorded using FANTASIO+ and have not yet been published. A portion of the spectrum for heavy water is presented in Figure 7. Although the 2CH spectral structure resembles a linear-type one, the present analysis was performed using an asymmetric-top Hamiltonian rather than a linear one as in the literature, thus accounting for all lines and making the linewidth analysis reported in Section 7 more reliable. The difference in linewidth with nearby C_2H_2 monomer lines is striking and will be discussed later.

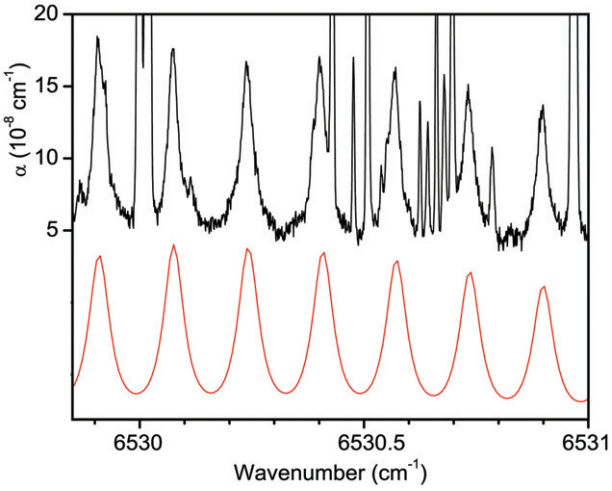

Figure 7. CW-CRDS jet-cooled spectrum of C_2H_2–D_2O recorded in the 2CH acetylenic excitation range using FANTASIO+. A portion of the P-branch is presented, observed (top) and simulated (bottom) with $T_{rot} = 20$ K. The C_2H_2–D_2O van der Waals was generated by expanding C_2H_2/Ar/D_2O 45/4500/0.1 sccm, p_0/p_∞ 70000/2 Pa through a 20×0.050 mm slit nozzle. D_2O was seeded into the gas mixture by saturating about 5% of the C_2H_2/Ar mixture (at 24°C) with D_2O by passing it through a 30 cm long bubbler filled with liquid D_2O (99.85% stated purity, Eurisotop). The expansion was sampled ~5 mm below the nozzle with a 134 µs typical ring-down time using a 10 mW TDL emitting in the 6520–6540 cm^{-1} wavelength range (Lucent M-D2525P58).

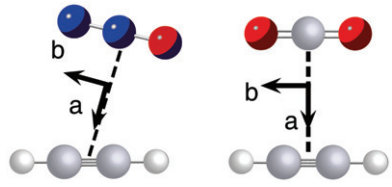

Figure 8. Geometries for C_2H_2–N_2O (left) and C_2H_2–CO_2 (right) as determined from microwave [102] and infrared [95] investigations, respectively.

4.2. CO_2 and N_2O

CO_2 and N_2O are isoelectronic and known to present close similarities when forming complexes with acetylene, in particular. They have parallel and slipped parallel geometries, respectively, as illustrated in Figure 8. In agreement with the axis-system reported in this figure, dominant b-type, with ΔK_a and ΔK_c odd and $\Delta J = 0, \pm 1$, selection rules are expected in C_2H_2–CO_2 and C_2H_2–N_2O, for 2CH vibrational excitation.

The C_2H_2–CO_2 complex has been previously investigated experimentally in both microwave [94] and mid-infrared [95] ranges and by *ab initio* methods [96–98], and also discussed within the context of Titan [99]. C_2H_2–N_2O was similarly investigated in the microwave [100–102] and in the mid-infrared [103,104] regions.

We successfully searched for the 2CH acetylenic excitation band in C_2H_2–CO_2 [105] and C_2H_2–N_2O [106] using FANTASIO(+). We even succeeded in observing the 2CH + torsion band in both species [107], inspired by similar observations in the lower energy spectral range [103,104,108]. One should note that calibration errors were later noticed for these combination bands and corrected in [109], with the origin of the 2CH + torsion band eventually some 44.5 cm^{-1} above the main band. FANTASIO+, only working in CW operation at the time, thus allowed a triple excitation band to be observed. Despite torsion being excited, corresponding to out-of-plane

intermolecular motion preparing the dimer on a more predissociative coordinate, sharp lines were observed, as illustrated for C_2H_2–CO_2 in Figure 9.

The spectrum of 2CH, C_2H_2–CO_2 shows numerous perturbations probably resulting from Coriolis-type mechanisms [105]. Together with the high line density, these many perturbations prevented us from reliably determining the rotational temperature, removing this dimer from the list of those complexes whose excited state lifetimes will be discussed in Section 7.

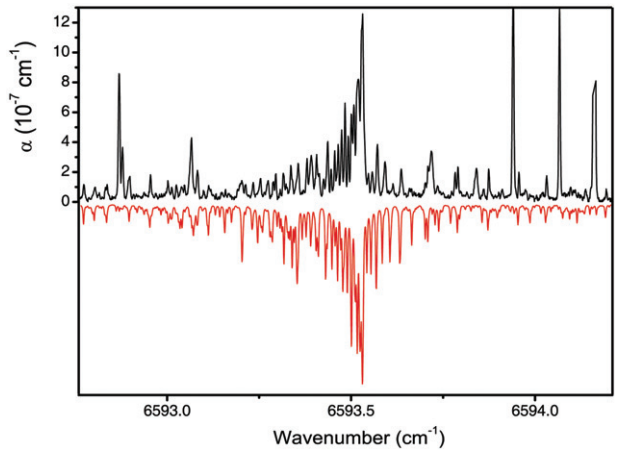

Figure 9. CW-CRDS jet-cooled spectrum of C_2H_2–CO_2 recorded in the 2CH acetylenic + torsion excitation range using FANTASIO(+). The central *Q*-branch is presented, observed (top) and simulated using the constants from [109] with $T_{rot} = 18$ K (bottom).

The published analysis on 2CH, C_2H_2–N_2O focused on the band center using a rigid rotor Hamiltonian [106]. We very recently succeeded in analyzing the very regular structures that were also initially recorded, away from the band center. A spectral portion showing newly identified lines, corresponding to this most recent work is shown in Figure 10. The analysis and the related rotational constants are detailed in [109]. It is interesting to highlight that, contrary to the 2CH, C_2H_2–CO_2 case study just mentioned, the 2CH, C_2H_2–N_2O band only shows small local perturbation and the rigid rotor model implemented in PGOPHER proved to be extremely successful [42].

5. Investigation of acetylene–acetylene complexes

5.1. $(C_2H_2)_2$

Acetylene is known to make homo-dimers [110], extensively investigated in the experimental and *ab initio* literature (see also e.g. [70,86,111–120]). They are today known to be T-shaped with ~2.7 Å hydrogen bond length and ~4.4 Å between centers of mass, as illustrated in Figure 11. We shall refer hereafter to the hat and body units of this T shape as identified in Figure 11. Trimers and tetramers have also been reported in the lower energy ranges, but much less extensively [121,122].

We noticed absorption features while recording C_2H_2–Ar spectra using FANTASIO(+) but could not

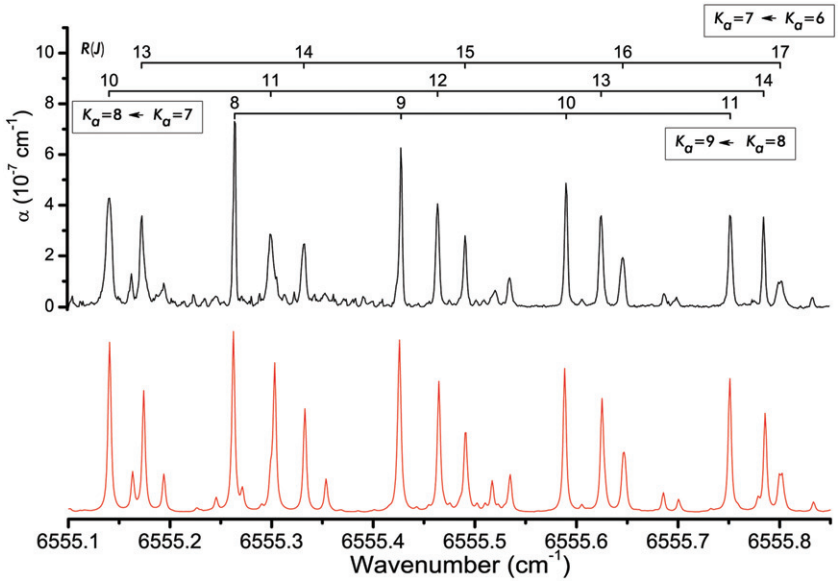

Figure 10. CW-CRDS jet-cooled spectrum of C_2H_2–N_2O recorded in the 2CH acetylenic excitation range using FANTASIO(+). A portion of the *b*-type *R*-branch is presented, observed (top) and simulated using the constants from [109] with $T_{rot} = 20$ K (bottom).

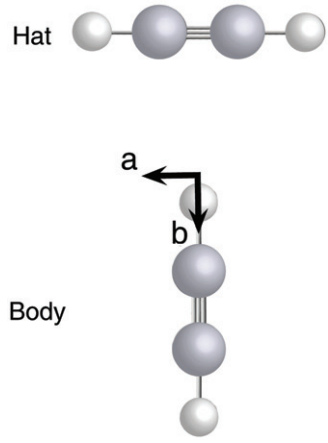

Figure 11. Geometry for $(C_2H_2)_2$ determined from microwave and infrared studies [112].

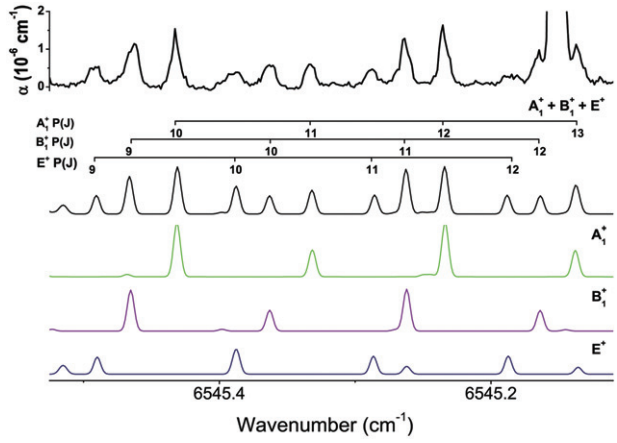

Figure 12. CW-CRDS jet-cooled spectrum of $(C_2H_2)_2$ recorded in the 2CH-hat acetylenic excitation range using FANTASIO+. A portion of the *P*-branch in the K_a–$K_a = 0$–1 sub-band is presented, observed (top spectrum) and simulated (bottom four spectra) with $T_{rot} = 23$ K. In the simulation, the three tunneling components are merged (middle spectrum) and separated (bottom three spectra).

assign them, initially. The favored chemical conditions were different than for C_2H_2–RG, becoming stronger when increasing acetylene relative to argon pressures. The structures also turned out to be present when using Ne and were soon identified to be $(C_2H_2)_2$ from the overall agreement between observed and simulated structures calculated using literature constants from lower energy states [112]. This identification was confirmed from a more detailed rotational analysis including the nuclear spin intensity alternation resulting from tunneling between the two acetylene units, as explained in a seminal paper in the literature [112]. The results are detailed in [46] and illustrated in Figure 12.

Interestingly, various types of 2CH excitation bands can be expected in the dimer, corresponding to two CH quanta in the hat or body units, or one CH quantum excitation simultaneously in each of the hat and body units. All of these were searched for but only the first two were identified.

2CH excitation in the hat unit is expected to lead to perpendicular, *b*-type selection rules, as illustrated for a sub-band in Figure 12. Several other sub-bands appear to be perturbed, some strongly, and further understanding will require merging experimental data and *ab initio* results, as for C_2H_2–Ar.

The band corresponding to 2CH excitation in the body unit is of parallel, *a*-type with ΔK_a even, ΔK_c odd and $J = 0, \pm 1$. Lines are strongly overlapped in this range avoiding any refinement from the analysis published in [46] to be suggested here.

5.2. $(C_2H_2)_n$

Larger C_2H_2 multimers, also called clusters and oligomers, have also been reported in the literature,

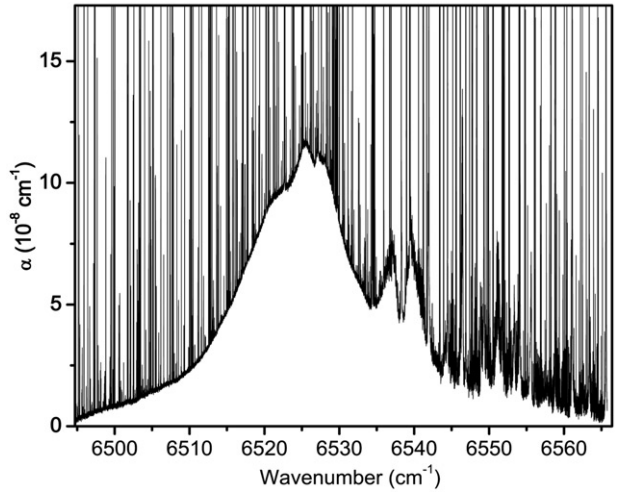

Figure 13. CW-CRDS jet-cooled spectrum of C_2H_2 multimers recorded in the 2CH acetylenic excitation range using FANTASIO+. The multimer band is the broad absorption feature centered around 6525 cm^{-1}. Absorption bands from the C_2H_2 dimer are also present, including *a*- (with *Q*-branch at 6538 cm^{-1}) and *b*-types (most features above 6540 cm^{-1}). The multimer was generated by expanding C_2H_2/Ar 185/2929 sccm, p_0/p_∞ 126000/2.5 Pa, slit nozzle 10 × 0.03 mm.

from spectra in the 3 μm range [123–126], as well as for C_2D_2 in the 4.17 μm range [120]. The former spectra are all broad and unstructured while that of the deuterated isotopologue is fully resolved. Increasing the C_2H_2 pressure using FANTASIO+ led us to observe very broad and barely structured absorption bumps in the 2CH range, as shown on Figure 13.

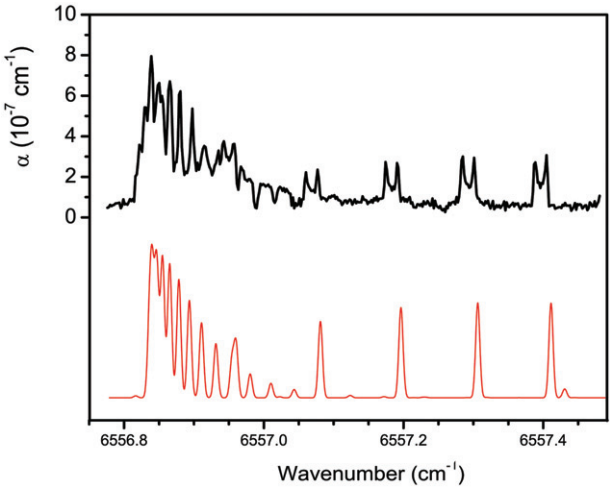

Figure 14. CW-CRDS jet-cooled spectrum of a mixture of $^{12}C_2H_2$ and Ar recorded in the 2CH acetylenic excitation range using FANTASIO(+), observed (top) and simulated (bottom). The simulation does not account for the line doubling attributed to a Doppler shift resulting from the specific repartition of C_2H_2–Ar in the circular nozzle expansion.

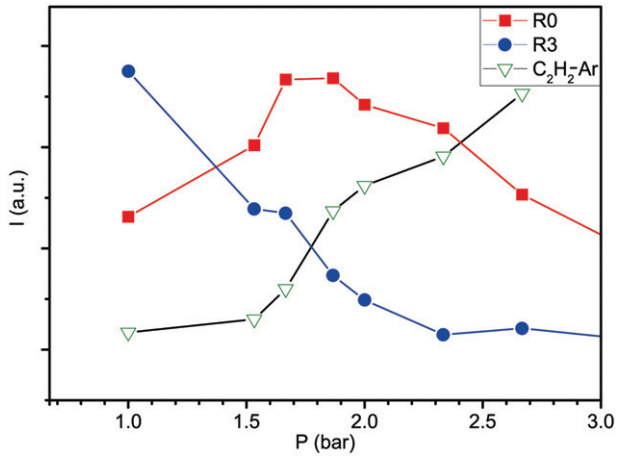

Figure 15. Variation with increasing argon carrier gas pressure of the $R(0)$ and $R(3)$ line intensities in the 2CH band of C_2H_2 cooled in a free jet expansion, recorded using CW-CRDS in FANTASIO+. The simultaneous intensity evolution of a line arising from $K_a = 0$ in C_2H_2–Ar is also presented. Acetylene input flow is very small and constant in all experiments (0.02 sccm). Pulsed circular nozzle operation is used.

We have, so far, been unable to further characterize these overtone, broad features, which are reported here for the first time in the literature. Although they have been observed with C_2H_2 seeded in either argon or neon, it cannot be excluded that the carrier species also contains some of the RG used in the expansion. Similar broad features have been reported for CO_2 clusters [127].

6. Further results from C_2H_2–Ar

6.1. *Spatial distribution*

Information about the spatial distribution in the free jet expansion was obtained for C_2H_2–Ar. We noticed unexpected features when comparing spectra recorded using slit and circular nozzles. As shown in Figure 14, lines in C_2H_2–Ar are double when using the circular nozzle and single with the slit nozzle. This was attributed to a Doppler shift indicating that this dimer is mainly present on the edge of the conical-shaped circular nozzle expansion [128]. The spectrum in Figure 14 is newly recorded using the recently installed pulsed nozzle. We also previously reported [128] and have since confirmed that C_2H_2 monomer lines simultaneously recorded with C_2H_2–Ar lines using circular nozzle expansion exhibit a central dip. This central position corresponds to zero Doppler shift, probably indicating that more efficient cluster formation occurs along the main axis of the expansion, reducing the concentration of cold monomer in this specific area of the expansion. Experiments have been carried out to provide more details on the related mechanism, but without definite results yet.

6.2. *Dimer formation*

Very recently, we attempted producing C_2H_2–Ar as rotationally cold as possible by increasing the argon carrier gas pressure in the jet. The C_2H_2 pressure was kept as low as possible to avoid detection saturation, and great care was taken to keep it constant during the experiments. As illustrated in Figure 15, the intensity of the $R(3)$ line in the 2CH band of the monomer keeps decreasing with increasing argon pressure. The rotational temperature is expected to decrease with increasing carrier gas pressure and this result indicates that the population on the lower $J = 3$ level is indeed decreasing together with rotational temperature, as expected. As shown in this figure, the population of $J = 0$ in the monomer, monitored through the $R(0)$ line intensity, is on the contrary increasing. This is also expected since all population ends up on $J = 0$. Ortho/para nuclear considerations that might affect this statement are probably not to be accounted for since C_2H_2–Ar is not fully symmetric (see discussion on intensity alternation in Section 3.1). This trend looks, however, to be soon balanced by another mechanism, now leading to the decrease of the $R(0)$ line intensity.

The threshold for this change is observed around $P = 2$ bar. It could be due to the formation of C_2H_2–Ar, which occurs precisely at the same threshold pressure, as revealed by the evolution of the intensity of lines in the dimer ($Q(2)$ from $K_a = 0$ in the complex was selected for Figure 15). As a result the gas heats up in the expansion, preventing the jet from further cooling down and thus probably inverting the population trend on $J = 0$ in the C_2H_2 monomer. The threshold temperature is around 4 K (T_{rot} in the monomer). This happens to be just above the predicted limit for which nuclear spin isomerization in the jet could possibly be highlighted [129,130]. These preliminary results will trigger further experiments using FANTASIO+.

6.3. *Perturbations through linewidths*

Linewidths appeared to be an interesting probe for local perturbations. One should remember that the probe laser beam in FANTASIO(+) is parallel to the slit nozzle, leading to sub-Doppler resolution, as further discussed in the next section. Anomalous, i.e. larger by a factor up to 6, FWHM values were observed for a number of lines in C_2H_2–Ar [66]. Close correspondence was found for pairs of $R(J-1)$ and $P(J+1)$ lines, supporting spectral assignment and pointing out upper J-level perturbation. This is illustrated in Figure 16, which highlights related series of R and P lines showing different, but upper level consistent line broadenings. Similar observations were made during the more recent analysis of C_2H_2–N_2O spectra referred to in Section 4.2, which are not detailed here.

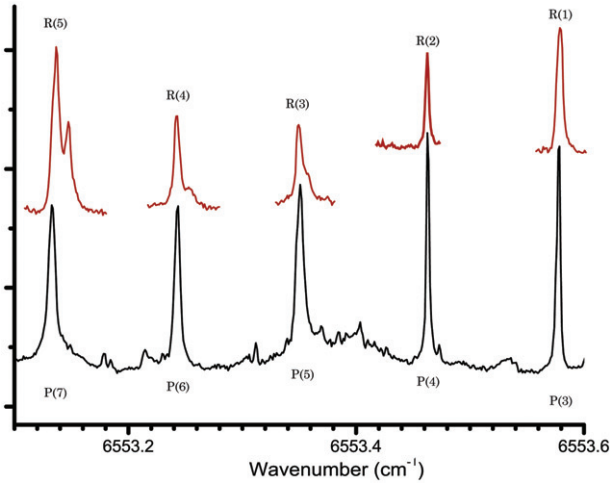

Figure 16. CW-CRDS jet-cooled spectrum of a mixture of $^{12}C_2H_2$ and Ar recorded in the 2CH acetylenic excitation range using FANTASIO(+). Related R and P lines in the 0–1, K_a sub-band are shown, demonstrating different but upper J-level consistent line broadening (see text).

7. Linewidth analysis

7.1. *Determining predissociation half-lifetimes*

When using a slit nozzle in FANTASIO+, the contribution of the Doppler effect to the line shape is expected to be very limited. It partly results from gas exiting at the edges of the slit at some angle. Neglecting this contribution as well as the instrumental linewidth, one can retrieve some information concerning lifetimes. The procedure is as follows: One first estimates T_{rot} from the evolution of relative line intensities in the rotational branches; then the intrinsic Doppler contribution to the line profile is calculated; next, the Lorentzian FWHM linewidth ($\Delta\nu^L_{FWHM}$) is retrieved; finally, molecular lifetimes are extracted using

$$\Delta\nu^L_{FWHM} = \frac{1}{2\pi}\left(\frac{1}{\tau_0} + \frac{1}{\tau_1}\right) \tag{4}$$

In this expression, $\tau_{0/1}$ is the mean lifetime in the ground/excited vibrational state, with τ_0 taken as ∞. It thus corresponds, in the absence of local perturbations, to the upper state predissociation half-lifetime.

All values resulting from 2CH excitation studies in acetylene containing molecular complexes are listed in Table 1. This table includes previously unpublished values resulting from the line shape analysis of the spectra we have reported here for the first time in the literature. The change in linewidth is illustrated in Figure 17.

7.2. *Trends in predissociation half-lifetimes*

We plotted the typical Lorentzian linewidth ($\Delta\tilde{\nu}^L_{FWHM}$) for the various investigated complexes against their

Table 1. Band origin shifts ($\Delta\nu$), with respect to the 2CH band in C_2H_2, predissociation lifetimes (τ_{2CH}) and calculated ground state interaction energies (D_e) of acetylene-containing van der Waals dimers excited in their 2CH vibrational state (see text for a more precise definition).

Complex	$\Delta\nu$ (cm^{-1})	τ_{2CH} (ns)	D_e (cm^{-1})
HCCH–Ar	−1.00	7.5	−122 [63]
HCCH–Kr	−1.38	–	−152 [40]
HCCH–N_2	−3.59	0.5	−275 [90]
HCCH–N_2O	−6.55	1.6	−570 [103]
HCCH–CO_2	−7.17	–	−810 [103]
HCCH–HCCH	Hat: −8.86 Body: −18.14	Hat: 1.0 Body: <0.5	−548 [119]
HCCH–D_2O	−27.74	0.17	–
HCCH–H_2O	−28.09	0.05	−1004 [91]

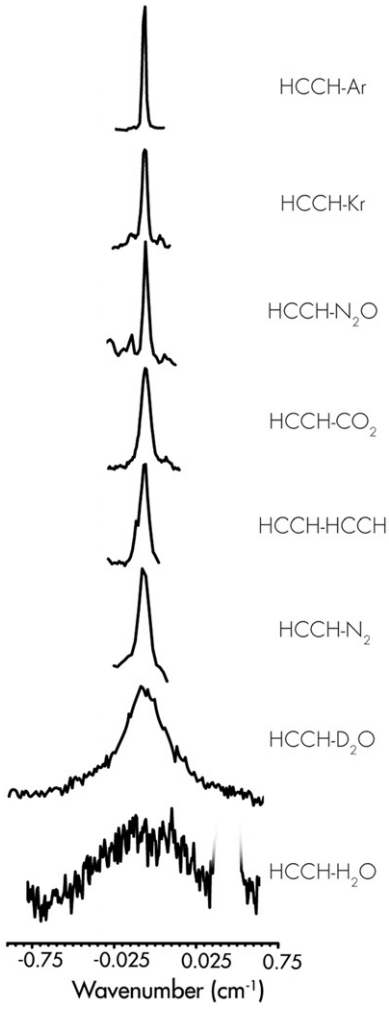

Figure 17. Illustration of the change in Lorentzian linewidth for the various investigated acetylene-containing van der Waals complexes in the 2CH excitation range.

band origin shifts ($\Delta\tilde{\nu}^0$). These shifts are calculated following Equation 5.

$$\Delta\tilde{\nu}^0 = \tilde{\nu}^0_{\text{complex}} - \tilde{\nu}^0_{C_2H_2} \tag{5}$$

where $\tilde{\nu}^0_{\text{complex}}$ is the band origin of the van der Waals complex and $\tilde{\nu}^0_{C_2H_2}$ is that of the C_2H_2 monomer (6556.47 cm^{-1} [49]). The result is presented in Figure 18, however, not directly including values for C_2H_2–CO_2 and C_2H_2–Kr for which T_{rot} could not be properly determined, as previously discussed. Actually, ln $\Delta\tilde{\nu}^L_{FWHM}$ is plotted. A linear trend is observed (see, however, the discussion around HF-containing complexes in [8]). Only C_2H_2–N_2 shows significant discrepancy from this behavior, possibly due to extensive perturbations as previously mentioned. One can actually predict $\Delta\tilde{\nu}^L_{FWHM}$ for C_2H_2–CO_2 (87 MHz) and

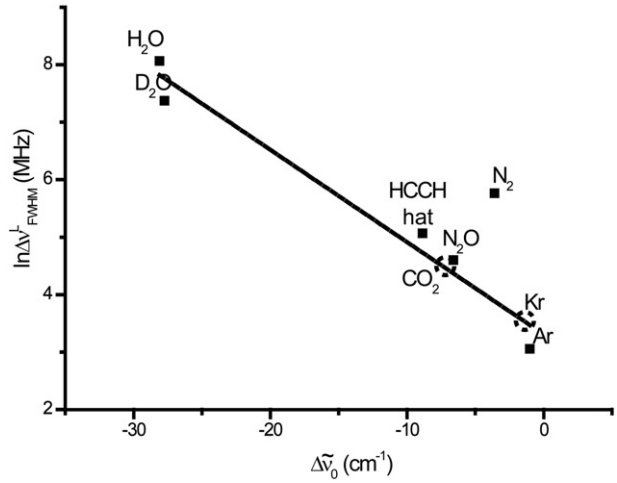

Figure 18. Logarithm of the predissociation FWHM versus the 2CH vibrational band origin shift for the different acetylene-containing van der Waals complexes being reported (see text for further details). Filled squares indicate known sets of values and empty circles refer to unknown linewidths (see text for further details).

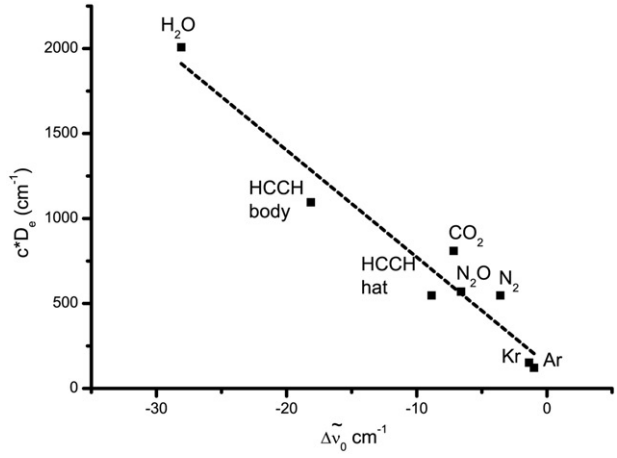

Figure 19. Empirical relation between van der Waals dissociation energy and the 2CH vibrational band origin shifts. *C* is a geometrical factor (see text for further details).

C_2H_2–Kr (34 MHz) from the corresponding values of $\Delta\tilde{\nu}^0$ known from spectral analyses and assuming a linear trend.

The vibrational band origin shift, $\Delta\tilde{\nu}^0$, is also usually correlated to the van der Waals interaction energy, D_e. We attempted to find a relation between these quantities, using literature values for D_e (see Table 1). The linear trend demonstrated in Figure 19 involves introducing a ''geometrical'' factor, *C*. It is taken as 2 if the 2CH excitation is oriented towards the van der Waals bond and as 1 if it is perpendicular.

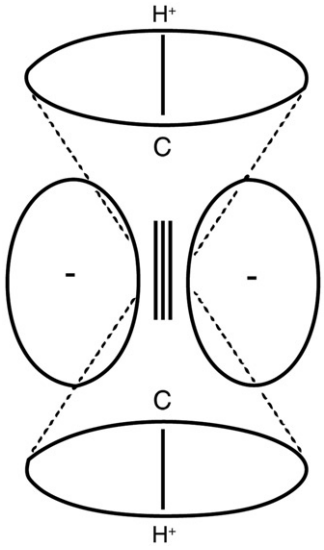

Figure 20. Picture of the elementary charge distribution in acetylene.

In the case of the dimer, $C=1$ or 2 was selected depending on whether dealing with the body or hat excitation. This most empirical relationship, which could be severely affected by large uncertainties on the D_e values, remains to be fully confirmed. Unfortunately, data on ν_3 in C_2H_2 monomer and complexes cannot be used for this purpose because they are affected by the $\nu_3/\nu_2+\nu_4+\nu_5$ anharmonic resonance [131]. Further relations, such as evidenced for HF hydrogen-bonded systems [132] cannot be applied to 2CH excited acetylene complexes because of the lack of appropriate data.

8. Conclusion

We have presented and discussed results concerning 2CH vibrational excitation in van der Waals complexes containing acetylene (C_2H_2). The related spectra were recorded around 1.5 μm using the FANTASIO(+) set-up that was described at the beginning of this paper. The various previously published results have been reviewed. Some of them have been updated. Also, unpublished results have been presented. Some of the major results were compared, those related to line-widths and vibrational band shifts, in particular.

Figure 20 displays the elementary charge repartition in acetylene, giving rise to an electric quadrupole moment. Accordingly, one can consider acetylene-containing van der Waals complexes either as ''H-bonded'' or ''π-bonded'' with respect to the acetylene moiety. According to the present results, H-bonded systems seem to present systematically smaller lifetimes in the 2CH vibrational excitation range. Also, it was demonstrated that H-bonded and π-bonded systems show different correlation between the van der Waals bond strength and the vibrational shift, the former set leading to an apparently smaller so-called geometrical factor, as defined in Figure 19. These various comparisons and statements, however, need further support and deeper explanation before being confirmed and possibly extended towards more van der Waals complexes, including those containing acetylene.

The main conclusion of this work certainly remains the amazing observation of well-resolved spectra of van der Waals dimers way above their dissociation limit. This result, which was only reported for a limited number of van der Waals complexes in the previous literature (see introduction), was obtained for the many probed dimers, except acetylene–helium. It thus seems to be almost the rule in the case of acetylene-containing molecular complexes. It is hoped that the present results, made possible because of the quality of the FANTASIO(+) experimental set-up, will stimulate the field of highly vibrationally excited molecular complexes, still in its infancy.

Acknowledgments

We thank the following people (cited in alphabetical order) for collaborating on various aspects of the work presently reviewed: Dr. P. Čermák (Lille and Bratislava), Dr. L. Coudert (Paris-Est), Dr. J. Demaison (Lille), Professor R. Georges (Rennes), Dr. W.J. Lafferty (Gaithersburg), Professor C. Leforestier (Montpellier), Dr. P. Macko (ULB and now JRC Ispra research center), Dr. A. Perrin (Paris-Est), Professor R.J. Saykally (Berkeley), Dr. C. Western (Bristol), and also, from ULB, X. de Ghellinck d'Elseghem Vaernewijck, B. Kizil, A. Rizopoulos, P. Van Poucke, and Dr. J. Vander Auwera.

Financial support along the years from EU, ULB, FRS-FNRS and the Fédération Wallonie-Bruxelles (ARC project) is acknowledged.

References

[1] A. Watanabe and H.L. Welsh, Phys. Rev. Lett. **13**, 810 (1964).
[2] D.D. Nelson Jr, G.T. Fraser and W. Klemperer, Science **238**, 1670 (1987).
[3] R.E. Miller, Science **240**, 447 (1988).
[4] A.J. Huneycutt and R.J. Saykally, Science **299**, 1329 (2003).
[5] J.N. Oliaee, M. Dehghany, N. Moazzen-Ahmadi and A.R.W. McKellar, Phys. Chem. Chem. Phys. **13**, 1297 (2011).
[6] A.C. Legon and D.J. Millen, Chem. Rev. **86**, 635 (1986).

[7] A. Weber, *Structure and Dynamics of Weakly Bound Molecular Complexes* (Dordrecht, Reidel, 1987).
[8] D.J. Nesbitt, Chem. Rev. **88**, 843 (1988).
[9] P.E.S. Wormer and A. van der Avoird, Chem. Rev. **100**, 4109 (2000).
[10] Y. Xu, W.J. Van and W. Jaeger, Int. Rev. Phys. Chem. **24**, 301 (2005).
[11] S. Davis, F. Dong and D.J. Nesbitt, in *Low Temperatures and Cold Molecules*, edited by I.M. Smith (Imperial College Press, London, 2008), pp. 231–294.
[12] A.R.W. McKellar, Ap. J. **326**, 75 (1988).
[13] W. Klemperer and V. Vaida, Proc. Natl. Acad. Sci. USA **103**, 10584 (2006).
[14] M. Herman and R.J. Saykally, Mol. Phys. **108**, 2153 (2010).
[15] I.V. Ptashnik, K.P. Shine and A.A. Vigasin, J. Quant. Spectrosc. Radiat. Transfer **112**, 1286 (2011).
[16] V. Vaida, J. Chem. Phys. **135**, 020901/020901 (2011).
[17] H.C. Chang, F.M. Tao, W. Klemperer, C. Healey and J.M. Hutson, J. Chem. Phys. **99**, 9337 (1993).
[18] C.-C. Chuang, K.J. Higgins, H.C. Fu and W. Klemperer, J. Chem. Phys. **112**, 7022 (2000).
[19] K. Von Puttkamer and M. Quack, Chimia **39**, 358 (1985).
[20] M.A. Suhm, J.T.J. Farrell, A. McIlroy and D.J. Nesbitt, J. Chem. Phys. **97**, 5341 (1992).
[21] D.T. Anderson, S. Davis and D.J. Nesbitt, J. Chem. Phys. **105**, 4488 (1996).
[22] M. Hippler, L. Oeltjen and M. Quack, J. Phys. Chem. **111**, 12659 (2007).
[23] H. Meyer, E.R.T. Kerstel, D. Zhuang and G. Scoles, J. Chem. Phys. **90**, 4623 (1989).
[24] S.A. Nizkorodov, M. Ziemkiewicz, D.J. Nesbitt and A.E.W. Knight, J. Chem. Phys. **122**, 194316 (2005).
[25] Z.S. Huang and R.E. Miller, J. Chem. Phys. **89**, 5408 (1988).
[26] R. Neuhauser, J. Braun, H.J. Neusser and A. van der Avoird, J. Chem. Phys. **108**, 8408 (1998).
[27] K.M. Beck, M.T. Berry, M.R. Brustein and M.I. Lester, Chem. Phys. Lett. **162**, 203 (1989).
[28] P. Medley, Z. Yu, B. Connors, W. Klemperer, S.N. Tsang and C.-C. Chuang, J. Chem. Phys. **124**, 214314/214311 (2006).
[29] Z. Yu, C.-C. Chuang, P. Medley, T.A. Stone and W. Klemperer, J. Chem. Phys. **120**, 6922 (2004).
[30] A.R.W. McKellar, J. Chem. Phys. **105**, 2628 (1996).
[31] M. Herman, K. Didriche, D. Hurtmans, B. Kizil, P. Macko, A. Rizopoulos and P. Van Poucke, Mol. Phys. **105**, 815 (2007).
[32] K. Didriche, C. Lauzin, T. Földes, X. de Ghellinck D'Elseghem Vaernewijck and M. Herman, Mol. Phys. **108**, 2155 (2010).
[33] D. Romanini, *Cavity-Ringdown Spectroscopy: A New Technique for Trace Absorption Measurements* (American Chemical Society, Washington, DC, 1998).
[34] G. Berden, R. Peeters and G. Meijer, Int. Rev. Phys. Chem. **19**, 565 (2000).
[35] B. Amyay, M. Herman, A. Fayt, A. Campargue and S. Kassi, J. Mol. Spectrosc. **267**, 80 (2011).
[36] M. Herman, Mol. Phys. **105**, 2217 (2007).
[37] M. Herman, in *Handbook of High Resolution Spectroscopy*, edited by M. Quack and F. Merkt (John Wiley & Sons, Chichester, UK, 2011), pp. 1993–2025.
[38] P. Macko, C. Lauzin and M. Herman, Chem. Phys. Lett. **445**, 113 (2007).
[39] A.P. Milce, D.E. Heard, R.E. Miller and B.J. Orr, Chem. Phys. Lett. **250**, 95 (1996).
[40] C. Lauzin, E. Cauët, J. Demaison, M. Herman, H. Stoll and J. Liévin, Mol. Phys., FASE special issue (2012).
[41] D.J. Nesbitt and R. Naaman, J. Chem. Phys. **91**, 3801 (1989).
[42] PGOPHER, a Program for Simulating Rotational Structure, C.M. Western, University of Bristol, UK, http://pgopher.chm.bris.ac.uk
[43] D. Romanini, A.A. Kachanov and F. Stoeckel, Chem. Phys. Lett. **270**, 546 (1997).
[44] P. Macko, D. Romanini, S.N. Mikhailenko, O.V. Naumenko, S. Kassi, A. Jenouvrier, V.G. Tyuterev and A. Campargue, J. Mol. Spectrosc. **227**, 90 (2004).
[45] W.H. Press, B.P. Flannery, S.A. Teukolsky and W.T. Vetterling, *Numerical Recipes. The Art of Scientific Computing* (Cambridge University Press, Cambridge, 1987).
[46] K. Didriche, C. Lauzin, T. Földes, D. Golebiowski, M. Herman and C. Leforestier, Phys. Chem. Chem. Phys., doi: 10.1039/c1cp2059561g (2011).
[47] P. Cermàk, Ph.D. thesis, Université J. Fourier (Grenoble, France) and Comenius University (Bratislava, Slovakia), 2010.
[48] K. Nakagawa, T. Katsuda, A.S. Shelkovnikov, M. De Labachelerie and M. Ohtsu, Opt. Commun. **107**, 369 (1994).
[49] Q. Kou, G. Guelachvili, M. Abbouti Temsamani and M. Herman, Can. J. Phys. **72**, 1241 (1994).
[50] P.N. Bajaj, R.K. Talukdar, P.K. Chakraborti and V.B. Kartha, J. Mol. Struct. **194**, 117 (1989).
[51] A. Fayt, S. Robert, G. Di Lonardo, L. Fusina, F. Tamassia and M. Herman, J. Chem. Phys. **126**, 114303 (2007).
[52] R.G.A. Bone, J. Phys. Chem. **98**, 3126 (1994).
[53] Z. Kisiel, J. Phys. Chem. **95**, 7605 (1991).
[54] C.R. Le Sueur, A.J. Stone and P.W. Fowler, J. Phys. Chem. **95**, 3519 (1991).
[55] A.E. Thornley and J.M. Hutson, Chem. Phys. Lett. **198**, 1 (1992).
[56] R.J. Bemish, P.A. Block, L.G. Pedersen, W. Yang and R.E. Miller, J. Chem. Phys. **99**, 8585 (1993).
[57] M. Yang and R.O. Watts, J. Chem. Phys. **100**, 3582 (1994).
[58] F.-M. Tao, S. Drucker and W. Klemperer, J. Chem. Phys. **102**, 7289 (1995).

[59] M. Yang, M.H. Alexander, H.-J. Werner and R.J. Bemish, J. Chem. Phys. **105**, 10462 (1996).
[60] T.H. Dunning Jr, J. Chem. Phys. **90**, 1007 (1989).
[61] R.A. Kendall, T.H. Dunning and R.J. Harrison, J. Chem. Phys. **96**, 6796 (1992).
[62] R.D. Hasse, M.W. Severson, M.M. Szczesniak, G. Chalasinski, P. Cieplak, R.A. Kendall and S.M. Cybulski, J. Mol. Struct. **436–437**, 387 (1997).
[63] C.R. Munteanu and B. Fernandez, J. Chem. Phys. **123**, 014309 (2005).
[64] D. Cappelleti, M. Bartolomei, M. Sabido, F. Pirani, G. Blanquet, J. Walrand, J.-P. Bouanich and F. Thibault, J. Phys. Chem. A **109**, 8471 (2005).
[65] D. Cappelletti, M. Bartolomei, E. Carmona-Novillo, F. Pirani, G. Blanquet and F. Thibault, J. Chem. Phys. **126**, 064311/1-10 (2007).
[66] C. Lauzin, K. Didriche, P. Macko, J. Demaison, J. Liévin and M. Herman, J. Phys. Chem. **113**, 2359 (2009).
[67] R.L. DeLeon and J.S. Muenter, J. Chem. Phys. **72**, 6020 (1980).
[68] Y. Ohshima, M. Iida and Y. Endo, Chem. Phys. Lett. **161**, 202 (1989).
[69] Y. Liu and W. Jäger, J. Mol. Spectrosc. **205**, 177 (2001).
[70] Y. Ohshima, Y. Matsumoto, M. Takami and K. Kuchitsu, Chem. Phys. Lett. **152**, 116 (1988).
[71] Y. Ohshima, Y. Matsumoto, M. Takami and K. Kuchitsu, Reza Kagachu Kenkyu **11**, 7 (1989).
[72] Y. Ohshima, Y. Matsumoto, M. Takami and K. Kuchitsu, J. Chem. Phys. **99**, 8385 (1993).
[73] T.A. Hu, D.G. Prichard, L.H. Sun, J.S. Muenter and B.J. Howard, J. Mol. Spectrosc. **153**, 486 (1992).
[74] R.J. Bemish and R.E. Miller, Chem. Phys. Lett. **281**, 272 (1997).
[75] C. Lauzin and K. Didriche, Phys. Chem. Chem. Phys. **13**, 751 (2011).
[76] R.J. Bemish, L. Oudejans, R.E. Miller, R. Moszynski, T.G.A. Heijmen, T. Korona, P.E.S. Wormer and A. van der Avoird, J. Chem. Phys. **109**, 8968 (1998).
[77] Y. Liu and W. Jaeger, Phys. Chem. Chem. Phys. **5**, 1744 (2003).
[78] U. Buck, I. Ettischer, S. Schlemmer, M. Yang, P. Vohralik and R.O. Watts, J. Chem. Phys. **99**, 3494 (1993).
[79] R. Moszynski, P.E.S. Wormer and A. van der Avoird, J. Chem. Phys. **102**, 8385 (1995).
[80] T.G.A. Heijmen, R. Moszynski, P.E.S. Wormer, A. van der Avoird, A.D. Rudert, J.B. Halpern, J. Martin, W.B. Gao and H. Zacharias, J. Chem. Phys. **111**, 2519 (1999).
[81] M. Rezaei, N. Moazzen-Ahmadi, A.R.W. McKellar, B. Fernández, and D. Farrelly, Mol. Phys., FASE special issue (2012).
[82] A.C. Legon, A.L. Wallwork and P.W. Fowler, Chem. Phys. Lett. **184**, 175 (1991).
[83] K.I. Peterson and W. Klemperer, J. Chem. Phys. **81**, 3842 (1984).
[84] R.D. Beck, A.G. Maki, S.H. Tseng and R.O. Watts, J. Mol. Spectrosc. **158**, 306 (1993).
[85] I. Hünig, L. Oudejans and R.E. Miller, J. Mol. Spectrosc. **204**, 148 (2000).
[86] C. Lauzin, N. Moazzen-Ahmadi and A.R.W. McKellar, J. Mol. Spectrosc. **269**, 124 (2011).
[87] P.A. Block, M.D. Marshall, L.G. Pedersen and R.E. Miller, J. Chem. Phys. **96**, 7321 (1992).
[88] P.A. Block, M.D. Marshall, L.G. Pedersen and R.E. Miller, J. Chem. Phys. **98**, 10107 (1993).
[89] M. Rezaei, N. Moazzen-Ahmadi and A.R.W. McKellar, J. Mol. Spectrosc. **272**, 19 (2012).
[90] D.J. Wales, A.J. Stone and P.L.A. Popelier, Chem. Phys. Lett. **240**, 89 (1995).
[91] D. Tzeli, A. Mavridis and S.S. Xantheas, J. Chem. Phys. **112**, 6178 (2000).
[92] D. Tzeli, A. Mavridis and S.S. Xantheas, J. Phys. Chem. A **106**, 11327 (2002).
[93] K. Didriche, C. Lauzin and T. Földes, Chem. Phys. Lett. **530**, 31 (2012).
[94] J.S. Muenter, J. Chem. Phys. **90**, 4048 (1989).
[95] Z.S. Huang and R.E. Miller, Chem. Phys. **132**, 185 (1989).
[96] R.G.A. Bone and N.C. Handy, Theor. Chim. Acta **78**, 133 (1990).
[97] W.B. De Almeida, Chem. Phys. **141**, 297 (1990).
[98] J.S. Muenter, J. Chem. Phys. **94**, 2781 (1991).
[99] C.C. Wang, P. Zielke, O.F. Sigurbjörnsson, C. Ricardo Viteri and R. Signorell, J. Phys. Chem. A **113**, 11129 (2009).
[100] H.O. Leung, Chem. Commun. **22**, 2525 (1996).
[101] H.O. Leung, J. Chem. Phys. **107**, 2232 (1997).
[102] R.A. Peebles, S.A. Peebles, R.L. Kuczkowski and H.O. Leung, J. Phys. Chem. **103**, 10813 (1999).
[103] T.A. Hu, L.H. Sun and J.S. Muenter, J. Chem. Phys. **95**, 1537 (1991).
[104] M. Dehghany, M. Afshari, O.J. Norooz, N. Moazzen-Ahmadi and A.R.W. McKellar, Chem. Phys. Lett. **473**, 26 (2009).
[105] C. Lauzin, K. Didriche, J. Liévin, M. Herman and A. Perrin, J. Chem. Phys. **130**, 204301 (2009).
[106] K. Didriche, C. Lauzin, P. Macko, M. Herman and W.J. Lafferty, Chem. Phys. Lett. **469**, 35 (2009).
[107] C. Lauzin, K. Didriche, T. Földes and M. Herman, Mol. Phys. **109**, 2105 (2011).
[108] C. Lauzin, J. Norooz Oliaee, M. Rezaei and N. Moazzen-Ahmadi, J. Mol. Spectrosc. doi: 10.1016/j.jms.2011.01.008 (2011).
[109] K. Didriche, T. Földes, C. Lauzin and M. Herman, Mol. Phys., FASE special issue (2012).
[110] R.D. Pendley and G.E. Ewing, J. Chem. Phys. **78**, 3531 (1983).
[111] D.G. Prichard, R.N. Nandi and J.S. Muenter, J. Chem. Phys. **89**, 115 (1988).
[112] G.T. Fraser, R.D. Suenram, F.J. Lovas, A.S. Pine, J.T. Hougen, W.J. Lafferty and J.S. Muenter, J. Chem. Phys. **89**, 6028 (1988).

[113] S.J. Grabowski, Annu. Rep. Prog. Chem., Sect. C: Phys. Chem. **102**, 131 (2006).
[114] K. Matsumura, T. Tanaka, Y. Endo, S. Salto and E. Hirota, J. Phys. Chem. **84**, 1793 (1980).
[115] R.E. Miller, P.F. Vohralik and R.O. Watts, J. Chem. Phys. **80**, 5453 (1984).
[116] D.G. Prichard, R.N. Nandi, J.S. Muenter and B.J. Howard, J. Chem. Phys. **89**, 1245 (1988).
[117] Y. Ohshima, Y. Matsumoto, M. Takami and K. Kuchitsu, Chem. Phys. Lett. **147**, 1 (1988).
[118] P.A. Le, C. Sheehan, D. Talbi and J.B.A. Mitchell, J. Phys. B: At. Mol. Opt. Phys. **30**, 319 (1997).
[119] C. Leforestier, A. Tekin, G. Jansen and M. Herman, J. Chem. Phys. **135**, 234301 (2011).
[120] J. Norooz Oliaee, N. Moazzen-Ahmadi, and A.R.W. McKellar, Mol. Phys., FASE special issue (2012).
[121] D.G. Prichard, J.S. Muenter and B.J. Howard, Chem. Phys. Lett. **135**, 9 (1987).
[122] G.W. Bryant, D.F. Eggers and R.O. Watts, J. Chem. Soc. Faraday Trans. II **84**, 1443 (1988).
[123] T. Dunder and R.E. Miller, J. Chem. Phys. **93**, 3693 (1990).
[124] Y.-C. Lee, V. Venkatesan, Y.-P. Lee, P. Macko, K. Didriche and M. Herman, Chem. Phys. Lett. **435**, 247 (2007).
[125] S. Hirabayashi, N. Yazawa and Y. Hirahara, J. Phys. Chem. **107**, 4829 (2003).
[126] T. Leisner and R. Wagner, in *Fundamentals and Applications in Aerosol Spectroscopy*, edited by R. Signorell and J.P. Reid (CRC Press, Boca Raton, 2011), pp. 3–24.
[127] J. Thievin, Y. Cadudal, R. Georges and A.A. Vigasin, J. Mol. Spectrosc. **240**, 141 (2006).
[128] K. Didriche, C. Lauzin, P. Macko, W.J. Lafferty, R.J. Saykally and M. Herman, Chem. Phys. Lett. **463**, 345 (2008).
[129] A. Amrein, M. Quack and U. Schmitt, Z. Phys. Chem. **154**, 59 (1987).
[130] B. Amyay, A. Fayt and M. Herman, J. Chem. Phys. **135**, 234301 (2011).
[131] W.J. Lafferty and R.J. Thibault, J. Mol. Spectrosc. **14**, 79 (1964).
[132] Z. Yu, E. Hammam and W. Klemperer, J. Chem. Phys. **122**, 194311 (2005).